

Perikinetics and sludge study for the decontamination of petroleum produced water (PW) using novel mucuna seed extract

Matthew Menkiti^{1,2} · Ifechukwu Ezemagu² · Bernard Okolo³

Received: 21 June 2015 / Published online: 8 April 2016
© The Author(s) 2016. This article is published with open access at Springerlink.com

Abstract In this study, *Mucuna flagellipes* seed extract was applied in the coagulation–flocculation of produced water (PW). Process parameters such as pH, dosage, and settling time were investigated. Process kinetics was also studied. Instrumental characterization of mucuna seed (MS), mucuna seed coagulant (MSC), and post effluent treatment settled sludge (PTSS) were carried out. The optimum decontamination efficiency of 95 % was obtained at 1 g/L MSC dosage, PW pH of 2, and rate constant of 0.0001 (L/g/s). Characterization results indicated that MS, MSC, and PTSS were of network structure, primitive lattice, and thermally stable. It could be concluded that MSC would be potential biomass for the treatment of produced water under the experimental conditions.

Keywords Mucuna seed · Produced water · Coagulation–flocculation · Sludge · Perikinetics

Abbreviations

K_m	Menkonu coagulation–flocculation rate constant
K	Coagulation–flocculation reaction rate constant
K_R	von Smoluchowski coagulation constant
β_{BR}	Collision factor for Brownian transport

ε_p	Collision efficiency
$\tau_{1/2}$	Coagulation period/Half life
$E(\%)$	Coagulation–flocculation efficiency
R^2	Coefficient of determination
α	Coagulation–flocculation reaction order
$-r$	Coagulation–flocculation reaction rate
MS	Mucuna seed
MSC	Mucuna seed coagulant
PTSS	Post treated settled sludge
PW	Produced water
N_0	Concentration of turbidity particles at time $t = 0$
N_t	Concentration of turbidity particles at time, t

1 Introduction

The production of oil and gas is accompanied by significant production of water, commonly known as “produced water”. Although there is no report of environmental disaster of high magnitude associated with produced water disposal in Niger Delta region of Nigeria, it is nevertheless known that much of this waste fluid is discharged into the environment or re-injected into the wells (Ezemagu 2015).

Produced water (PW), highly turbid in nature, is generated during first stage of petroleum exploitation and/or as associated residual fluid during petroleum storage. Several physical and chemical factors affect the characteristics of produced water. These factors include, but are not limited to, humic acids content, suspended/dissolved organic and inorganic substances, pH, and temperature (Frost et al. 1998; Wang et al. 2014; Ezechi and Isa 2014).

Over the years, there has been increasing concerns for the environmental protection of aquatic systems receiving

✉ Matthew Menkiti
matthew.menkiti@ttu.edu; cmenkiti@yahoo.com

¹ Water Resources Center, Department of Civil and Environmental Engineering, Texas Tech University, Lubbock, TX, USA

² Department of Chemical Engineering, Nnamdi Azikiwe University, Awka, Nigeria

³ Department of Chemical Engineering, Michael Okpara University of Agriculture, Umudike, Nigeria

inadequately treated PW. In order to address these concerns, different treatment techniques have been employed. They include, but are not limited to, adsorption, microfiltration, photo-catalysis, ion exchange, reverse osmosis, oxidation, coagulation–flocculation and neutralization, dissolved air precipitation, biological degradation, nanofiltration, and ultra-filtration (Shubo et al. 2002; Jerry et al. 2011; Colberg et al. 2012; Bouaziz et al. 2014; Huang et al. 2014; Ezemagu 2015).

Among these technologies, coagulation–flocculation presents a superior viable primary treatment option for the PW. The advantages of coagulation–flocculation over other technologies are: (1) easy on-site implementation, (2) high treatment efficiency, (3) simplicity, and (4) low installation and operating costs (Karthik et al. 2008). Coagulation has always been the core effluent treatment process for removal of colloidal and organic/inorganic materials, which could cause color and turbidity (Choi et al. 2008; Ugurlu et al. 2008; Zheng et al. 2009; Wei et al. 2009; Menkiti and Onukwuli 2012; Okolo et al. 2014).

Coagulation entails addition of coagulant to water in order to neutralize the charges on the colloidal particles, thus eliminating the repulsive forces that keep the particles apart, so that the particles come close enough to stick together. The continuous multiple build-up of the sticking particles into visible settleable flocs is known as flocculation (Huang and Chen 1996; Tatsi et al. 2003).

The performance of the coagulation–flocculation process is largely affected by the coagulant type, raw effluent quality, temperature, pH, chemical and effluent's bacteriological characteristics etc. (Jin 2005; Menkiti et al. 2009). Chemical coagulants such as ferric chloride, calcium hydroxide, alum, ferric sulfate, ferrous sulfate, polyaluminum chloride, and lime (Amokrane et al. 1997; Graham et al. 2008; Yang et al. 2010; De Godos et al. 2011; Imran et al. 2012) have been widely used in removing a wide range of particles from wastewater. Nevertheless, these chemical coagulants have disadvantages, which include large volume of sludge resulting in huge disposal cost, not being effective in low-temperature water, and high procurement cost. Furthermore, aluminum-based coagulants are associated with Alzheimer disease in humans (Moraes 2004; Chen et al. 2010; Zhu et al. 2011).

Because of these inherent disadvantages of the chemical coagulants, search for alternative coagulants becomes imperative. Natural coagulants have attracted more attention due to their eco-friendliness. Natural coagulants are considered safe for human health, because they are biodegradable, natural, nontoxic, and renewable (Zhao et al. 2012; Rajab et al. 2013). These natural coagulants of plant origin include, but are not limited to, *Moringa oleifera*, Maize, Nirmali (*Strychnos potatorum*) seed, *Plantago psyllium*, *Plantago ovata*, *Hibiscus esculentus* seed pods,

Chestnut, *Jatropha curcas* seeds (Sen and Bulusu 1962; Tripathi et al. 1976; Raghuwanshi et al. 2002; Oluwalana et al. 2004; Mei Fong et al. 2014; Sciban et al. 2009). In this current work, extract from mucuna seed (MS), provided the focus for this study.

MS has been considered for use as a coagulant because it is biodegradable, nontoxic, and safe to human health. It also contains highly soluble proteins (Menkiti et al. 2010; Ugonabo et al. 2012; Ezemagu 2015). The application of either natural or mineral coagulants is associated with generation of sludge. The sludge generated during bio-coagulation has not yet been studied; a gap this work is attempting to close. An insight into the basic characteristics of the PTSS could provide vital information for possible wide application of the sludge. It could also give ideas on the treatment and disposal options available for PTSS. This study also extended into how process parameters would influence the effectiveness of mucuna seed coagulant (MSC) in the decontamination of PW, in addition to the study of the process kinetics.

2 Materials and methods

2.1 Material preparation and characterization

2.1.1 Produced water (PW)

The produced water was collected from a petroleum refinery located in Port Harcourt, Nigeria. The collected sample was stored and characterized on the bases of standard procedure (APHA 1999). The Chemical Oxygen Demand was determined by following the methodology (specific to high salt containing liquid waste) as described by APHA (1999). In accordance with the procedure, the digestion mixture was prepared by adding $K_2Cr_2O_7$, 3 g (which was previously dried at 103 °C for 2 h), to concentrated (18.4 M) H_2SO_4 , 167 mL and $HgSO_4$, 33 g, and made up to 500 mL with distilled water. The mixture was cooled to room temperature before it was diluted to 1000 mL. The sulfuric acid reagent (2.5 %, w/v) was prepared by dissolving Ag_2SO_4 in H_2SO_4 . The sampling of wastewater and digestion mixture of the sample was carried out in accordance with methodology described under the analysis of water and wastewater in the literature (APHA 1999).

2.1.2 Mucuna seed (MS)

The MS sample was bought from Eke-Aku market, Igbotiti, Enugu State, Nigeria. Distilled water was used to thoroughly wash the samples of MS, which was then sun dried for 10 days. The samples were processed to MSC

based on the modified procedure reported by Sutherland (2005). In this procedure, 100 g of sieved powdered MS was soaked in ethanol and the soaked mixture was continuously stirred using a magnetic stirrer for 2 h 30 min. Next, the mixture was filtered using Whatman filter paper no 3. The residue obtained after the filtration was transferred into a beaker containing 1:25 w/v mixture of complex salts (0.7 g/L CaCl₂, 4 g/L MgCl₂, 0.75 g/L KCl, 30 g/L NaCl) solutions. The mixture of residue and complex salt solution was stirred for 2 h using a magnetic stirrer. Then, it was filtered using Whatman filter paper in order to discard spent solid. The filtrate was poured in a sufficiently agitated beaker and heated at 70 °C for 2 min to precipitate out the needed biocoagulant from the filtrate solution. The precipitated biocoagulant (MSC) was poured into the specified filter paper(s) and allowed to dry at room temperature for 24 h to solid biocoagulant.

2.2 Coagulation–flocculation procedure

The coagulation–flocculation experiments were conducted using a jar test apparatus at room temperature and are described as follows.

2.2.1 Influence of dosage of MSC on removal efficiency

The initial turbidity was measured using a Digital Turbidimeter (model WZS-185, Japan). The pH of produced water (PW) was also recorded at room temperature. For each run, 1000 mL of PW samples were poured in ten different 1000 mL-GG-17 beakers. The desired dosages of MSC were between 0.5 and 5 g/L. The jar testing started when desired MSC dosages were put into PW samples contained in the 1000 mL beakers and rapid mixed at 250 rpm for 3 min. This was followed by slow agitation at 30 rpm for 40 min. After slow mixing, the treated PW samples were immediately transferred into 1000 mL Borex measuring cylinders. Then, each of the PW samples in the various cylinders was allowed to settle for 35 min. During the settling time, 15 mL of the supernatant (upper layer of the settling effluent) was pipetted from 3 cm depth into a 120 mL cuvette. Residual particle concentrations of supernatants were recorded. The residual particle concentration (in mg/L) was obtained as a product of residual turbidity (NTU) and conversion factor (T_f). T_f has a value of 2.35 (Metcalf and Eddy Inc 2003).

2.2.2 Influence of PW pH on removal efficiency

For the evaluation of the effect of pH, the optimum dosage of MSC obtained in Sect. 2.2.1 was used in the jar test as described below: the pH of PW was adjusted to desired pH using 0.1 M H₂SO₄ and 0.1 M NaOH just before dosing of

the MSC. After the adjustment, MSC samples with optimum dosage were separately put into eight beakers containing 1000 mL PW, and subsequently rapid mixed (250 rpm) for 3 min and slow mixed (30 rpm) for 40 min using a magnetic stirrer. After the slow mixing, each of the treated PW sample was allowed to settle for 30 min. During settling time, 15 mL of the supernatant was withdrawn from 3 cm depth and measured for particle concentration (mg/L) at the specified pH.

2.2.3 Influence of time on removal efficiency

First, an optimum amount of MSC was put into a beaker containing 1000 mL PW. Then, the mixture of PW and MSC was rapid mixed at 250 rpm for 3 min, and then slow mixed at 30 rpm for 40 min, using a magnetic stirrer. Finally the treated PW was allowed to settle for 30 min. During settling period, the particle concentrations were determined at 3, 5, 10, 15, 20, 25, and 30 min using conversion factor of 2.35.

2.3 Instrumental characterization

The precursor (MS), biocoagulant (MSC), and settled sludge (PTSS) were characterized using the following instruments: (i) Thermo Nicolet Nexus 470/670/870FTIR unit (Thermo Nicolet Corporation, USA), (ii) Zeiss EVO[®]MA 15 EDX/WDS unit (Zeiss, USA) (surface morphology), (iii) PHILIPS X PERT X-RAY diffraction unit (PANalytical, USA) with Cu Kr radiation (30 kV and 30 mA) at a scan rate of 1°/min (XRD), (iv) TGA-Q50 and DSC-Q200 unit (TA Instruments, USA) (Thermal stability).

3 Kinetics theory and model development for coagulation process

3.1 The Brownian coagulation theory

In an aqueous suspension, where Brownian motion dominates, the number of collision occurring per unit time per unit volume, K_{xy} , for two particles of volumes V_x and V_y is expressed as (von Smoluchowski 1917; Liyang 1988; Holthof et al. 1996; Menkiti et al. 2010):

$$K_{xy} = \beta_{BR}(v_x v_y) n_x n_y, \quad (1)$$

where $\beta_{BR}(v_x v_y)$ is the Brownian aggregation collision frequency which depends on particle size, temperature, and pressure; $n_x n_y$ is the particle concentrations for two particles of sizes x and y .

The formation rate r_f of particles of volume v_p , as a result of collisions between particles of volumes v_x and v_y is expressed as (Liyang 1988; Okolo et al. 2014):

$$r_f = \frac{1}{2} \sum_{x+y=p} K_{xy} \tag{2}$$

Note that $x + y = p$ shows that the summation is governed by collisions, for which

$$v_x + v_y = v_p \tag{3}$$

In a reverse case, the dissociation rate of particles of volume v_p by collision with other particles is given as (Liyang 1988; Okolo et al. 2014):

$$r_1 = \sum_{x=1}^{\infty} K_{xk} \tag{4}$$

Hence, the rate of change in the number of density of particles of volume V_p is

$$\frac{dn_k}{dt} = r_f - r_1, \tag{5}$$

Substituting Eqs. (2) and (4) into Eq. (5), yields

$$\frac{dn_k}{dt} = \frac{1}{2} \sum_{x+y} \beta_{BR}(V_x V_y) n_x n_y - n_k \sum_{x=1}^{\infty} \beta_{BR}(V_x V_p) n_x \tag{6}$$

The collision frequency function can be obtained through the steady-state particle diffusion as:

$$k_{xy} = 4\pi(D_x + D_y)(a_x + a_y), \tag{7}$$

where $D_x + D_y = D_p$.

Thus Eq. (7) is simplified to:

$$k_{xy} = 4\pi(D_p)(a_x + a_y) \tag{8}$$

For a monodisperse system where particles of volume, $v_x = v_y$, the Einstein–Stokes relation could be expressed as Eq. (9) (Holthof et al. 1996):

$$D_x = \frac{KT}{6\pi\mu a_x} \text{ and } D_y = \frac{KT}{6\pi\mu a_y} \tag{9}$$

Hence the Einstein–Stokes equation is reduced to:

$$D_x = \frac{KT}{6\pi\mu} \left(\frac{1}{a_x} + \frac{1}{a_y} \right) \tag{10}$$

Inserting Eq. (10) into Eq. (8) yields:

$$K_{xy} = 4\pi \left(\frac{KT}{6\pi\mu} \left(\frac{1}{a_x} + \frac{1}{a_y} \right) (a_x + a_y) \right) \tag{11}$$

$$K_{xy} = \frac{2KT}{3\mu} \frac{(a_x + a_y)^2}{a_x + a_y} \tag{12}$$

For the collision frequency function of Eq. (12), for the case of monodisperse dimer formation, the following conditions apply:

$$\frac{(a_x + a_y)^2}{a_x a_y} = \begin{cases} 4 & \text{for } a_x = a_y \\ > 4 & \text{for } a_x \neq a_y \end{cases}$$

and for the case of $a_x = a_y$, Eq. (12) transforms to Eq. (13):

$$K_{11} = \frac{8KT}{3\mu}, \tag{13}$$

where K_{11} is the Von Smoluchowski coagulation rate constant.

Also for the case of $K_{xy} \rightarrow K_{11} = \beta_{BR}(v_x v_y) n_x n_y$, Eq. (6) is solved exactly to yield:

$$\frac{N_t}{N_0} = \frac{(K_{11} N_0 t / 2)^{n-1}}{(1 + K_{11} N_0 t / 2)^{n+1}} \tag{14}$$

It has been established for an aggregating system at $n = 1$; it could be extended into flocculation regime, such that

$K_{11} \approx K_m$ (Menkiti and Onukwuli 2012), and Eq. (14) transforms to Eq. (15):

$$\frac{1}{\sqrt{N_L}} = \left(\frac{K_m N_0}{\sqrt{2} N_0} \right) t + \frac{1}{\sqrt{N_0}}, \tag{15}$$

where $K_m = \frac{1}{2} \beta_{BR} = \frac{2}{3} \varepsilon_p \frac{K_{BT}}{\eta}$.

K_m is the Menkonu coagulation–flocculation rate constant accounting for Brownian coagulation–flocculation transport of destabilized particles at α th order. ε_p is the collision efficiency.

The coagulation–flocculation period is obtained from Eq. (14) as

$$t_{1/2} = \frac{1}{(0.5 K_m N_0)} \tag{16}$$

The physical significance of Eq. (16) is that it represents the time at which the initial total number of particles is reduced by half and it is therefore a coagulation time scale.

The coagulation–flocculation efficiency could be calculated using Eq. (17)

$$E(\%) = \left(\frac{N_0 - N_t}{N_0} \right) \times 100 \tag{17}$$

4 Results and discussion

4.1 Characterization results

4.1.1 Characteristics of produced water (PW)

The characteristics of PW are shown in Table 1. The conductivity value obtained in Table 1 showed that PW contained charged ions from different substances that made

Table 1 Characteristics of produced water (PW)

Parameter	Value	Unit
pH	8	
Fe ²⁺	0.711	mg/L
SO ₄ ²⁻	26	mg/L
NO ₃ ²⁻	12.8	mg/L
Alkalinity	1820.5	mg/L
Acidity	202	mg/L
Ca ²⁺	Nil	mg/L
Mg ²⁺	Nil	mg/L
Salinity	3842	mg/L
Turbidity	1435	NTU
Conductivity	12.17	ms/mc
Total dissolved solids	1899	mg/L
Total suspended solids	1473	mg/L
COD	10	mg/L
Hydrocarbon	99.7	ppm

Table 2 Proximate analysis results of mucuna seed

Parameter	Value	Unit
Bulk density	0.53	g/mol
Oil content	5.30	%
Ash content	2.80	%
Moisture content	11.0	%
Protein content	22.7	%
Weight loss	10.9	%
Yield	89.0	%

up the PW. The high turbidity of PW in Table 1 was due to the suspended solids which accounted for the cloudiness of the effluent. The values as represented in Table 1 were adequate to favor coagulation–flocculation treatment of PW.

4.1.2 Mucuna seed (MS)

Shown in Table 2 are the physiochemical parameters values of MS, such as yield (%), weight (%), bulk density (g/mL), ash content (%), oil content (%), moisture content (%), and protein content (%), which were obtained based on the standard AOAC methods (Atkins 1990). The calculated yield value depicted in Table 2 is significant to highlight the prospect of MS as a good precursor that could be processed into MSC.

4.1.3 FTIR spectra analyses of MS, MSC, and PTSS

The prevalent functional groups of MS, MSC, and PTSS were determined from Fig. 1 using spectra (4000–600 cm⁻¹) that

were compared to an FTIR library (Stuart 2004). Figure 1 shows the peaks of 3700–3500 cm⁻¹ for: (a) MS, (b) MSC, and (c) PTSS, and were attributed to O–H groups. The peaks in the range of 3288–3335 cm⁻¹ were attributed to secondary amide. An aliphatic ring was linked to the region of 2918–2850 cm⁻¹ for (a) MS (2919 cm⁻¹), (b) MSC (2918–2850 cm⁻¹), and (c) PTSS (2919–2850 cm⁻¹). The medium peaks range (1720–1528 cm⁻¹) are recorded for MSC (1623, 1558–1541 cm⁻¹ for NH₂) and PTSS (1558–1539 cm⁻¹ for N–H bending; C–N stretching and NO₂ asymmetric). Peaks at 1362, 1298, and 1284 cm⁻¹ were assigned to MS with SO₂ asymmetric stretching. Also, S=O stretching (1206 cm⁻¹), B–H bending (1020 cm⁻¹), and out of plane C–H bending (944–609 cm⁻¹) were for MS. Peaks at 1456, 1417, and 1488 cm⁻¹ denoted azo compound (N=N stretching) in MSC and PTSS. Bands for MSC at 897–945 cm⁻¹ and PTSS at 712–699 cm⁻¹ were attributed to C–H stretching.

4.1.4 SEM/elemental results of MS, MSC, and PTSS

Figures 2, 3, and 4 show the surface morphologies of MS, MSC, and PTSS. Two images (a, b), were obtained at different magnifications for each of Figs. 2, 3, and 4. Figure 2a for MS depicts the aggregated porous network structure of tender looking tissue. Figure 2b for MS depicts magnified, multiple aggregated networked pores that are evenly distributed. These pores are an initial indication of active sites for sticking of particles. Figure 3a for MSC shows more enlarged pores in the MSC. The multiple predominant pores characterized by rounded protrusions indicated added porosity after processing MS into MSC. Figure 4 for PTSS shows a highly compact and filled structure without voids. The filled pores indicated that the particles readily attached on the surfaces of the pores to form the sludge. The existence of the white region could be as a result of transfer of potassium-based compounds from effluent to MSC to form PTSS. Table 3 shows the elemental compositions of MS, MSC, and PTSS. Clearly the presence of elements, originally not seen in MSC, but subsequently present within PTSS matrix, was an indication of transfer of elements/particles from PW to the MSC.

4.1.5 XRD result of MS, MSC, and PTSS

The X-Ray diffraction for: (a) MS, (b) MSC, and (c) PTSS are depicted in Fig. 5. Figure 5a reveals the presence of broad peaks, indicating the poor crystalline nature of the MS sample. Figure 5b, for MSC shows five clear peaks while Fig. 5c for PTSS shows 12 clear peaks. The crystal peaks in Figs. 5b, c on comparison with the standard crystal peaks were shifted towards left–right axes, which

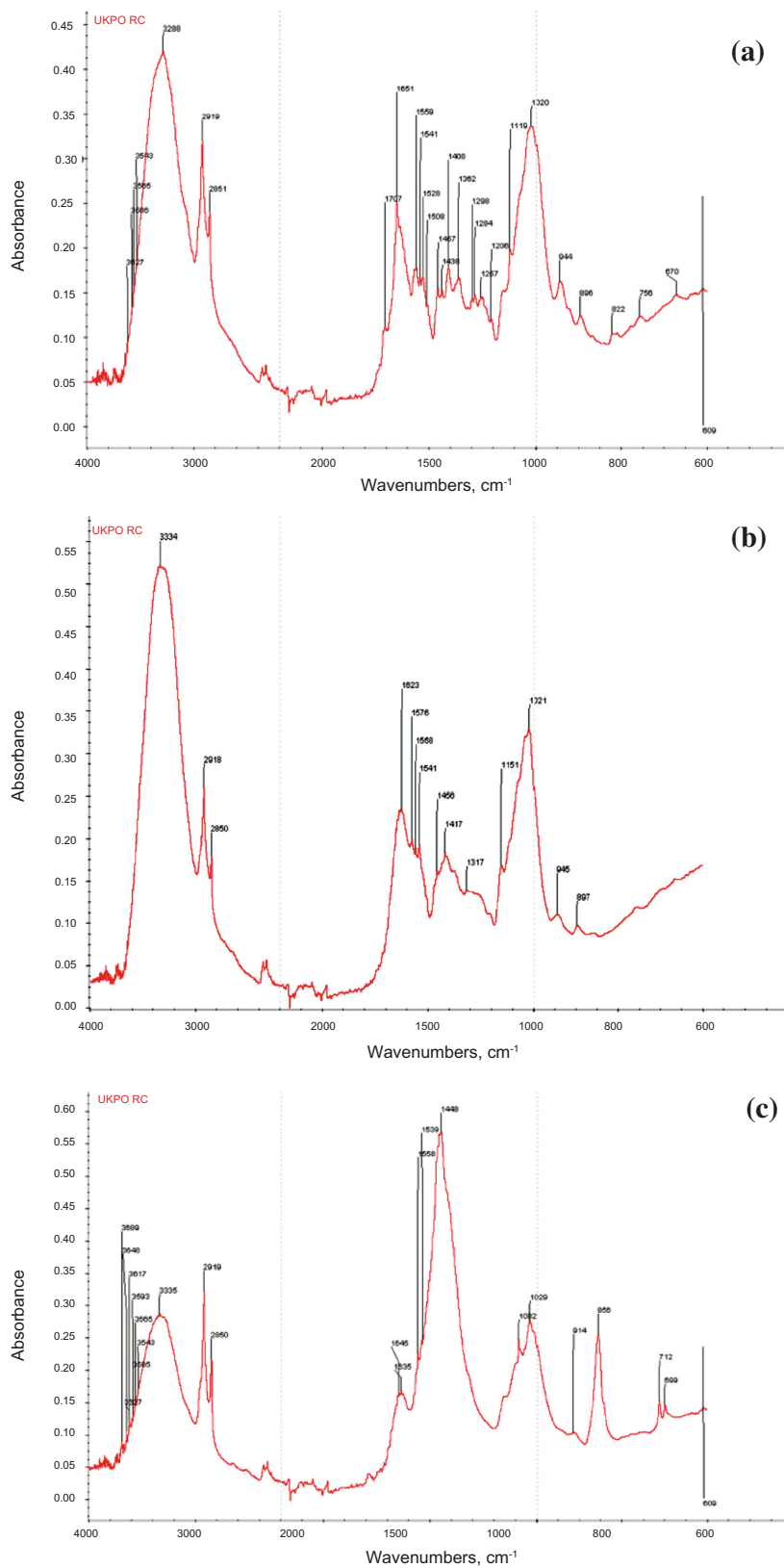


Fig. 1 FTIR spectra for **a** MS, **b** MSC, **c** PTSS

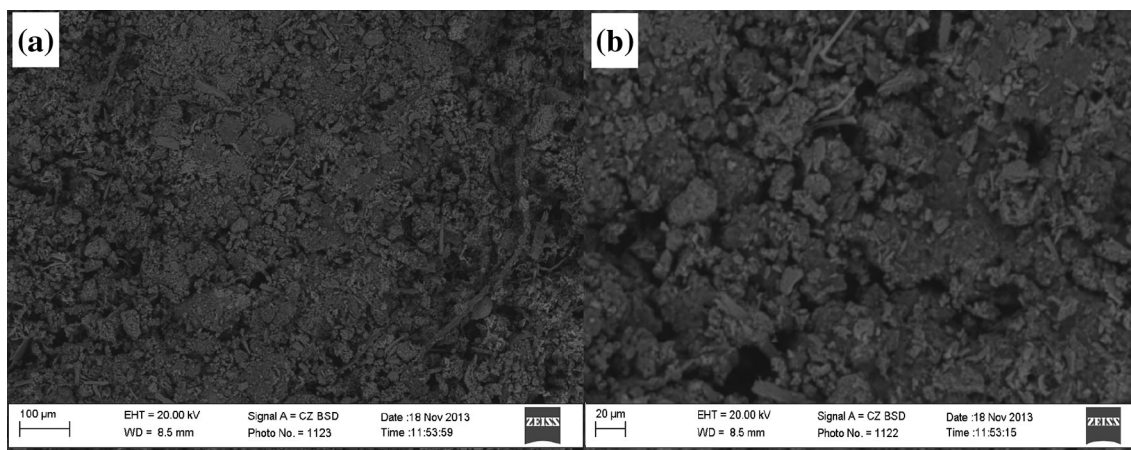


Fig. 2 SEM micrographs of MS

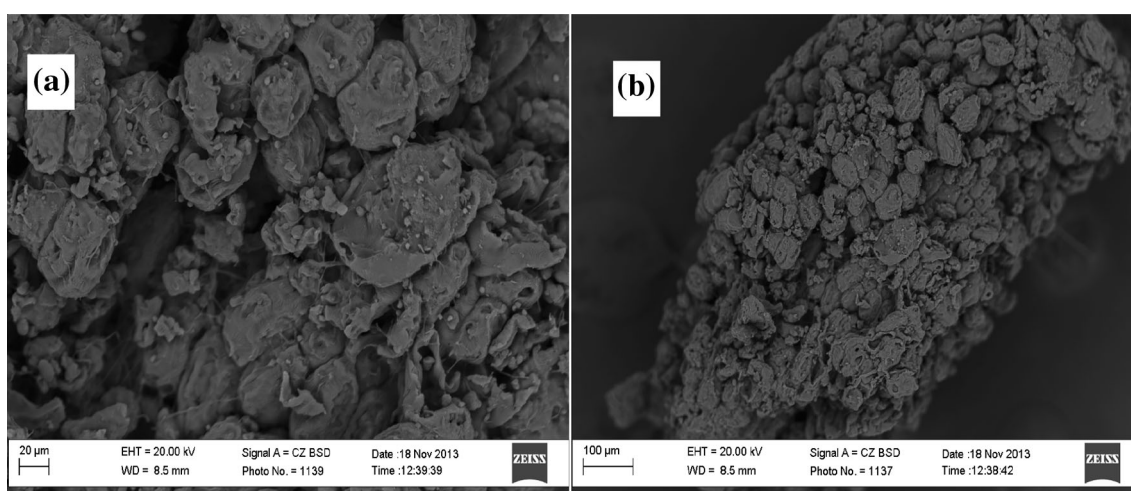


Fig. 3 SEM micrographs of MSC

might be the result of expansion or contraction of MSC (Ezema [2015](#)). Figure 5b, c indicated primitive lattice structure for MSC and PTSS, respectively. MS was poorly crystalline.

4.1.6 TGA/DSC of mucuna seed (MS), mucuna seed coagulant (MSC), and post treated settled sludge (PTSS)

These are analyses (TGA and DSC) that account for the thermal behavior of samples (Brukh and Mitra [2007](#); Vyazovkin [2012](#); Menkiti et al. [2014](#)). Figures 6, 7, and 8 show the TGA and DSC curves for MS, MSC, and PTSS. The thermograms shown in Fig. 6a (MS) and Fig. 7a (MSC) had final residual mass of 1.189 mg (27.5 % original mass) and 1.839 mg (60 % original mass), respectively. In Figs. 6a and 7a, the first weight losses resulted from internal moisture and gaseous losses from the samples

(Menkiti et al. [2014](#)). Furthermore, weight losses were linked to the decomposition of the labile component in both MS and MSC.

Phase transition occurred over the temperature ranges of 37.5–298 and 25–298 °C, with transition enthalpies of 13.779 and 11.8421 kJ/mol (Figs. 6b, 7b), respectively. Both Figs. 6b and 7b demonstrated the coiling of the long chain protein moiety, leading to spontaneous densification. At 125–298 and 162.5–298.5 °C, the densification occurred with absorption of thermal energy (Figs. 6b, 7b). This was an indication that the heat flow disks exhibited exothermicity.

Figure 8 shows the TGA/DSC of PTSS. Figure 8a for PTSS shows dehydration and volatilization that persisted till 262.5 °C, losing about 10 % (0.352 mg) of its weight (Verma et al. [2010](#); Ezema [2015](#)). Between 262.5–450 °C, the residue oxidized and lost about 15 % (0.88 mg) of its weight. At maximum 590 °C in Fig. 8a,

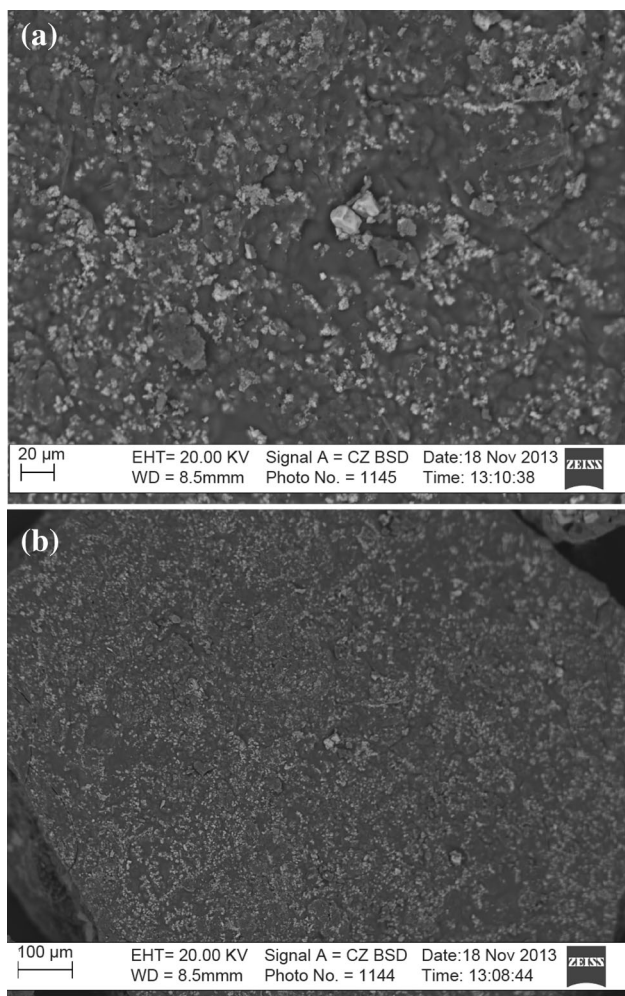


Fig. 4 SEM micrographs of PTSS

Table 3 Elemental composition of MS, MSC, and PTSS

Element, wt%	MS	MSC	PTSS
C	9.43	16.03	11.49
Na	8.24	2.75	18.13
Mg	0.19	0	1.47
Al	0	3	2.42
Si	0.2	0	3.99
P	0.43	0.57	0.52
S	0	6	1.36
Cl	39.14	2.3	10.97
K	24.17	0.43	0.6
Ca	7.19	41.56	20.06
Ti	0	3.73	0.19
Fe	0	0	2.95
Cu	0	0	0
O	11.01	23.63	25.85

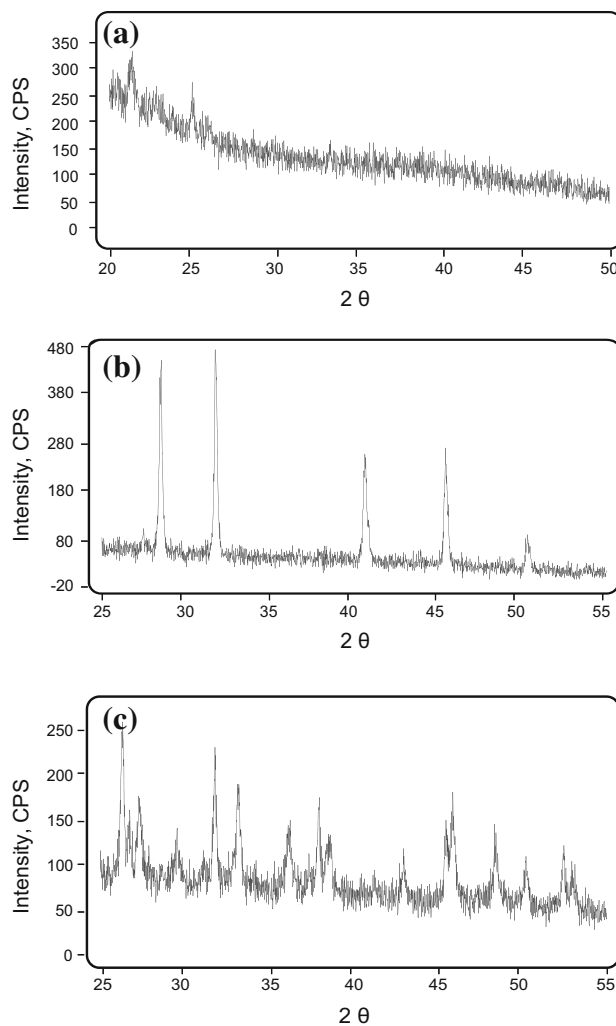


Fig. 5 XRD pattern of: **a** MS, **b** MSC, **c** PTSS

PTSS lost 1.1 mg of its initial mass (3.520 g). At 590 °C, oxidation and dehydration of sample were at maximum (Verma et al. 2010). The weight loss could be attributed to fragmentation or decomposition of labile components in the sample. The interactive effects of MSC with various chemical substances and particles contained in PW are shown as two eutectics downward peaks in Fig. 8b. The presence of the two peaks in Fig. 8b indicated that the components of the sample were not a single pure substance. However, Figs. 6, 7, and 8 indicated thermal stability.

4.2 Process factors influence

4.2.1 Effect of MSC dosage on particle removal efficiency

Figure 9 showed that the particle removal efficiency increased from 58.1 % at 0.5 g/L of MSC, reaching a maximum of 60 % (at 1 g/L of MSC) and thereafter

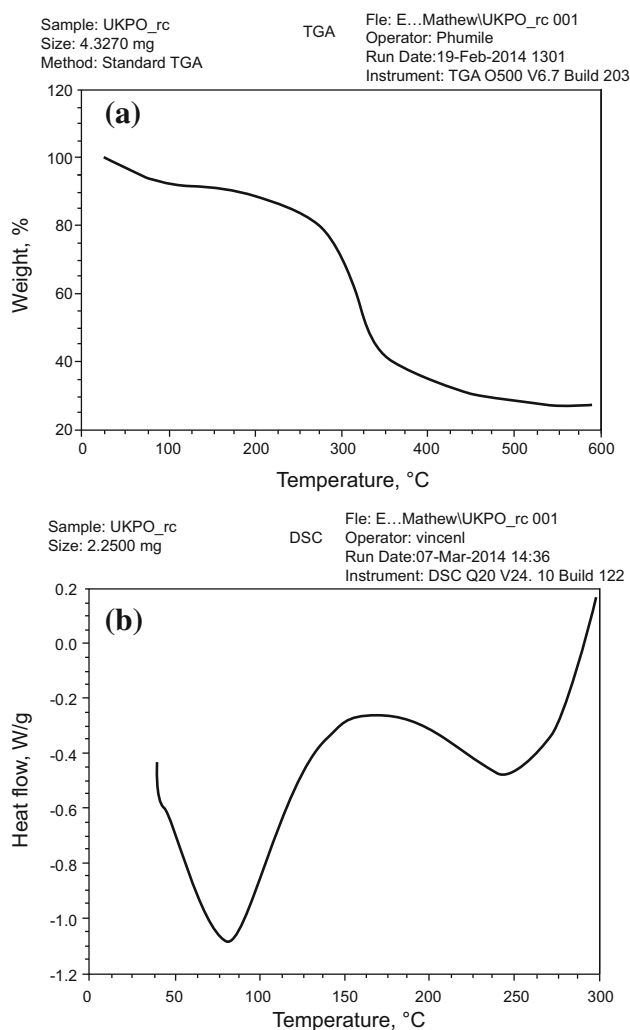


Fig. 6 Profile of **a** TGA and **b** DSC of MS

reduced to 52.9 % at 2.5 g/L. Minimum efficiency was recorded at 50.1 % for 5 g/L. The removal efficiency increase resulted from increased protonation of the fluid, which incrementally destabilized PW-charged species (mainly $-ve$ charges), leading to the particle removal efficiency increasing as MSC dosage increased from 0.5 to 1 g/L. The removal efficiency then declined with increasing MSC dosage (1.5–5 g/L). The decline resulted from sustained restabilization and returbidization following net protonation of the fluid after 1 g/L MSC dosing was exceeded. In this work, 1 g/L was adopted as optimal dosage and applied in the evaluation of pH effect in Sect. 4.2.2.

4.2.2 Effect of pH on particle removal at 1 g/L of MSC

Figure 10 shows the effect of pH, varied from 2–9, on particle removal. The profile in Fig. 10 indicated alternate decline and increment in performance as the pH changed

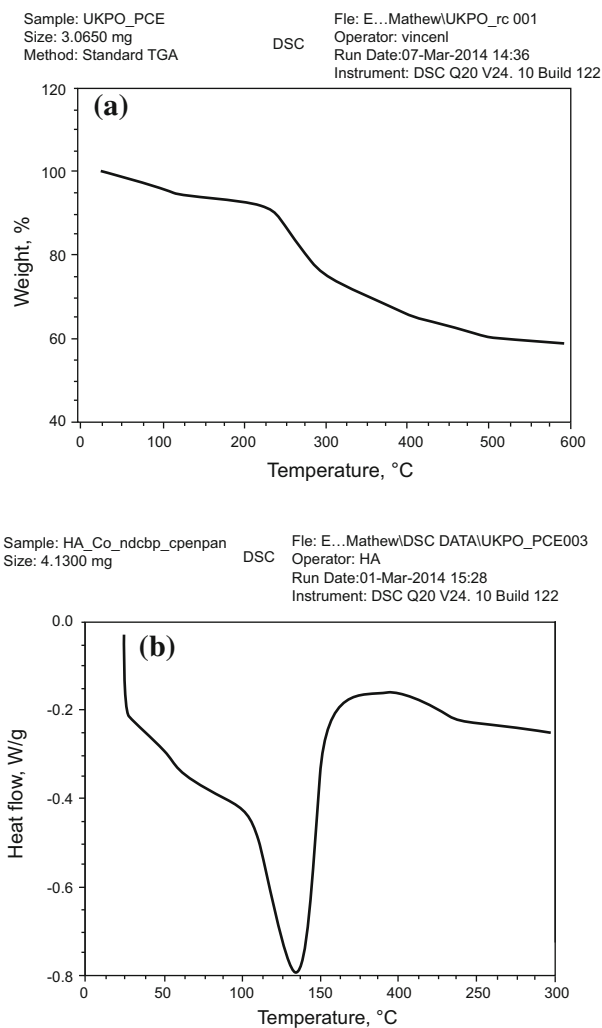


Fig. 7 Profile of **a** TGA and **b** DSC of MSC

from 9–2. The particle removal efficiency which rose in pH ranges of 3–2 and 7–5 could be linked to increased protonation of the fluid. Conversely, the declined in performance at pH ranges 9–7 and 5–3 could be linked to $+ve$ and $-ve$ species-induced charge reversal, respectively. The charge reversal occurred when either one of the charged species was in excess. The maximum removal efficiency of 84 % at pH 2 indicated a point of equilibrium in the concentrations of ions and counter-ions participating in the coagulation–flocculation process (Menkiti and Onukwuli 2012).

4.2.3 Variation of particle removal efficiency with time at 1 g/L of MSC and pH 2

The variation of particle removal efficiency with time at 1 g/L of MSC and pH 2 is shown in Fig. 11. Figure 11 shows that the particle removal efficiency gradually

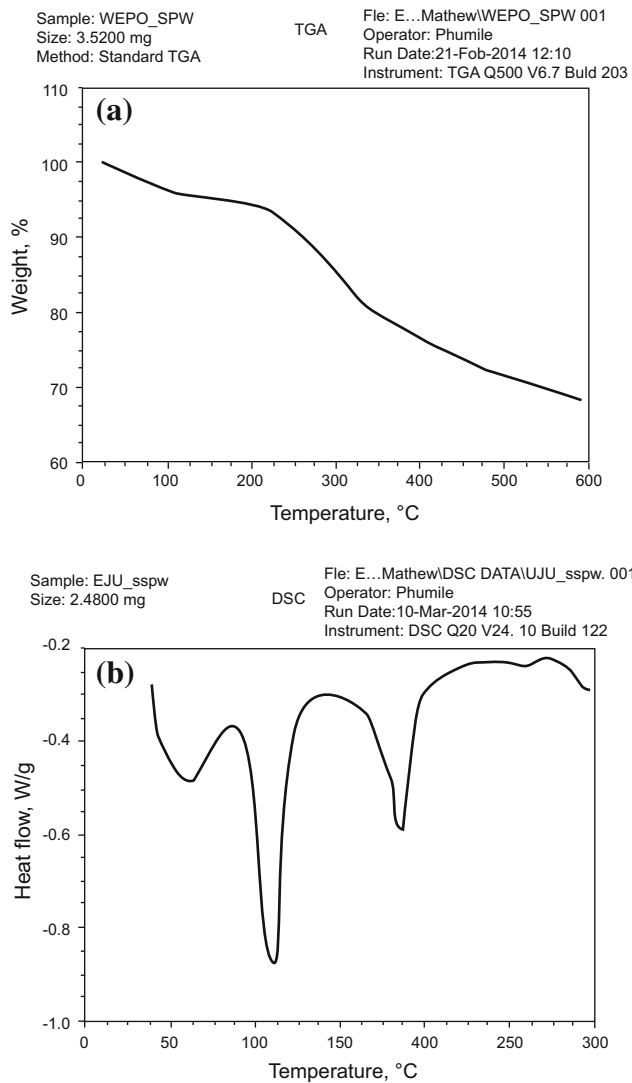


Fig. 8 Profile of a TGA and b DSC of PTSS

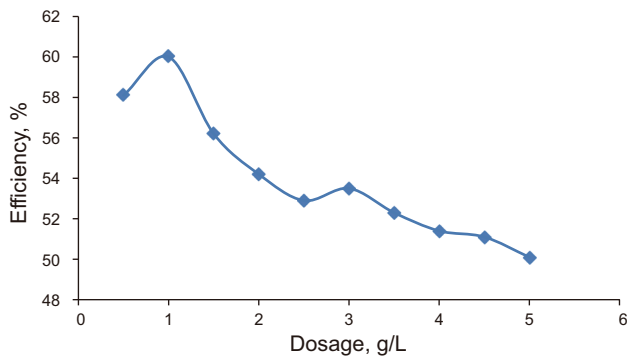


Fig. 9 Removal efficiency vs dosage for MSC in PW

increased with time until 20 min, after which the efficiency became stable. This indicates that performance equilibrated at 20 min.

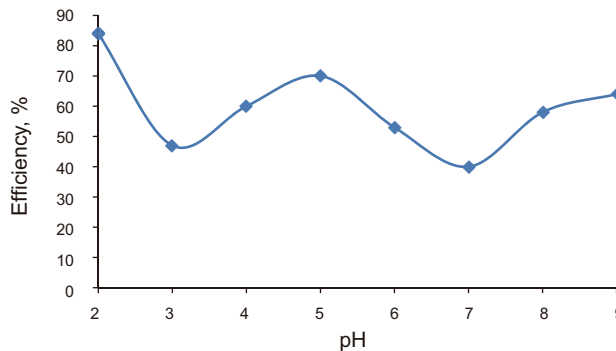


Fig. 10 Removal efficiency vs pH at 1 g/L

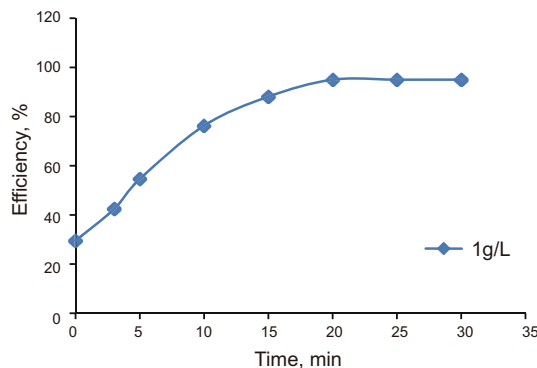


Fig. 11 Influence of time on efficiency at 1 g/L and pH 2

Table 4 Nephelometric kinetics parameters

Parameter	Value
K_m , L/g/s	0.0001
$\frac{1}{N_0}$, L/g	0.0015
N_0 , g/L	666.6
R^2	0.989
$\tau^{1/2}$, s	30.003
K_R , g ² /s	3.00E-10
β_{BR} , L/g/s	0.0002
$-r$	6.00E-07
D' , g ² /m/s	2.00E-05
α	2

4.3 Process kinetics

Table 4 displays nephelometric kinetics results evaluated at pH 2, 1 g/L of MSC, and an initial particle load of 3372 g/L. The overall rate constant K_m was obtained as a slope of the plot (plot not shown) of $\frac{1}{\sqrt{N_t}}$ vs t (Eq. 15), for the case of $\alpha = 2$. K_m is a vital parameter that indicates the speed of floc formation and it accounted for the aggregation process that started from initial coagulation to viable floc formation and subsequent settling. The higher the

value of K_m , the higher the efficiency in clarification. Preferentially, best results can be obtained at α range of 1–2 (Menkiti and Onukwuli 2012; Ugonabo et al. 2012). For the process kinetics, the value of R^2 indicates a second-order model for the perikinet process. For perikinetics, $2K_m = \beta_{BR}$. A high magnitude K_m translates to high kinetic energy necessary to reduce the zeta potential within the fluid medium. The result would be substantial reduction in double layer effects or improved colloidal destabilization at low $\tau_{1/2}$ (30.003 s) to enhance the high rate of process aggregation.

5 Conclusion

In this report, the performance of MS extract as an effective biocoagulant has been established at the conditions of this study. The process effectively removed 84 % of particle load from the PW effluent. Also, the study showed that dosage and pH had significant influence on the performance of MSC. Characteristics of MSC have shown biomass with sufficient active surface to be used as a biocoagulant. The sample would be also considered thermally stable. The sludge composition indicates it could be a resource for materials absorbed from the effluents.

Open Access This article is distributed under the terms of the Creative Commons Attribution 4.0 International License (<http://creativecommons.org/licenses/by/4.0/>), which permits unrestricted use, distribution, and reproduction in any medium, provided you give appropriate credit to the original author(s) and the source, provide a link to the Creative Commons license, and indicate if changes were made.

References

- Amokrane A, Comel C, Veron J. Landfill leachates pre-treatment by coagulation–flocculation. *Water Res.* 1997;31:2775–82.
- APHA (American Public Health Association), AWWA (American Water Works Association), WPCF (Water Pollution Control Federation). Standard methods for the examination of water and wastewater. Washington, DC: APHA; 1999.
- Atkins PW. Physical chemistry. 4th ed. Oxford: Oxford University Press; 1990.
- Bouaziz M, Gargouri B, Gargouri OD, et al. Application of electrochemical technology for removing petroleum hydrocarbons from produced water using lead dioxide and boron-doped diamond electrodes. *Chemosphere.* 2014;117:309–15.
- Bruk R, Mitra S. Kinetics of carbon nanotube oxidation. *J Mater Chem.* 2007;17:619–23.
- Chen T, Gao B, Yue Q. Effect of dosing method and pH on color removal performance and floc aggregation of polyferric chloride-polyamine dual-coagulant in synthetic dyeing wastewater treatment. *Colloids Surf A.* 2010;355:121–9.
- Choi KJ, Kim SG, Kim SH. Removal of antibiotics by coagulation and granular activated carbon filtration. *J Hazard Mater.* 2008;151:38–43.
- Colberg JS, Wang X, Goual L. Characterization and treatment of dissolved organic matter from oilfield produced water. *J Hazard Mater.* 2012;217–218:164–70.
- De Godos I, Guzman HO, Soto R, et al. Coagulation/flocculation-based removal of algal–bacterial biomass from piggery wastewater treatment. *Bioresour Technol.* 2011;102:923–7.
- Ezechi EH, Isa MH. Boron removal from produced water using electrocoagulation. *Proc Saf Environ Prot.* 2014;92:509–14.
- Ezemagu IG. Nephelometric study of adsorptive and non-adsorptive component of coagulation of produced water and paint effluent using bioextract. M.Sc. Thesis, Nnamdi Azikiwe University, Awka; 2015.
- Frost TK, Johnsen S, Utvik TI. Environmental effects of produced water discharges to the marine environment. OLF, Norway. 1998. <http://www.olf.no/static/en/rapporter/producedwater/summary.html>. Accessed 24 Aug 2015.
- Graham N, Gang F, Fowler J, Watts M. Characterization and coagulation performance of a tannin-based cationic polymer: a preliminary assessment. *Colloids Surf A.* 2008;327:9–16.
- Holthof H, Egelhaaf SU, Brorkovee M, et al. Coagulation rate measurement of colloidal particles by simultaneous static and dynamic light scattering. *Langmuir.* 1996;12:5541.
- Huang C, Chen Y. Coagulation of colloidal particles in water by chitosan. *J Chem Technol Biotechnol.* 1996;66:227–32.
- Huang X, Bo X, Zhao Y, et al. Effects of compound bioflocculant on coagulation performance and floc properties for dye removal. *Bioresour Technol.* 2014;165:116–21.
- Imran Q, Hanif MA, Riaz MS, et al. Coagulation/flocculation of tannery wastewater using immobilized chemical coagulants. *J Appl Res Technol.* 2012;10(2):79–86.
- Jerry N, Kenneth L, Elisabeth MD. Produced water: overview of composition, fates and effects. Environmental risks and advances in mitigation technologies. New York: Springer; 2011. p. 3–54.
- Jin Y. Use of a high resolution photographic technique for studying coagulation/flocculation in water treatment. M.Sc. Thesis, University of Saskatchewan, Saskatoon; 2005. p. 22–29.
- Karthik M, Dafale N, Pathe P, Nandy T. Biodegradability enhancement of purified terephthalic acid wastewater by coagulation–flocculation process as pretreatment. *J Hazard Mater.* 2008;154:721–30.
- Liyang L. Effect of surface chemistry on kinetics of coagulation of submicron iron oxide particles in water. Pasadena: W.M Keck Laboratory of Environmental Engineering Science, Division of Engineering and Applied Science, California Institute of Technology; 1988. p. 8–10.
- Mei Fong C, Chai SL, John R, et al. A review on development and application of plant based bioflocculants and grafted bioflocculants. *Ind Eng Chem Res.* 2014;53:18357–69.
- Menkiti MC, Nnaji PC, Onukwuli OD. Coag-flocculation kinetics and functional parameters response of periwinkle shell coagulant (PSC) to pH variation in organic rich coal effluent medium. *Nat Sci.* 2009;7(6):1–18.
- Menkiti MC, Nnaji PC, Nwonye CI, et al. Coag-flocculation kinetics and functional parameters response of mucuna seed coagulant to pH variation in organic rich coal effluent medium. *J Miner Mater Charact Eng.* 2010;2(8):89–103.
- Menkiti MC, Aneke MC, Ejikeme PM, et al. Adsorptive treatment of brewery effluent using activated *Chrysophyllum albidum* seed shell carbon. *SpringerPlus.* 2014;3:213.
- Menkiti MC, Onukwuli OD. Coag-flocculation of mucuna seed coag-flocculant (MSC) in coal washery effluent (CWE) using light scattering effects. *AIChE J.* 2012;8(4):1303–7.
- Metcalf and Eddy, Inc. Waste water engineering: treatment and reuse. 4th ed. New York: Tata-McGraw Hill; 2003.
- Moraes LCK. Estudo da Coagulação-Ultrafiltração com o Biopolímero Quitosana para a Produção de Água Potável. Dissertação de Mestrado. Programa de Pós-Graduação em Engenharia Química, Universidade Estadual de Maringá; 2004.
- Okolo BI, Menkiti MC, Nnaji PC, et al. The Performance of okra seed (*Hibiscus esculentus* L.) extract in removal of suspended

- particles from brewery effluent by coag-flocculation process. *Br J Appl Sci Technol*. 2014;4(34):4791–806.
- Oluwalana SA, Bolaji W, Martus GD, Alegbeleye O. Domestic water purification using *Moringa oleifera*. *Niger J For*. 2004; 29(1):28–32.
- Raghuwanshi PK, Meindloi MJ, Sharma AD, et al. Improving filtration quality using agrobased materials as coagulation aid. *Water Qual Res Can*. 2002;37(4):745–56.
- Rajab AH, Idrisa A, Abdullaha N, et al. Production and characterization of a bioflocculant produced by *Aspergillus flavus*. *Bioresour Technol*. 2013;127:489–93.
- Sciban M, Klasnja M, Anmtov M, et al. Removal of water turbidity by natural coagulants obtained from chestnut and acorn. *Bioresour Technol*. 2009;100(24):6639–43.
- Sen AK, Bulusu KR. Effectiveness of Nirmali seed as coagulant and coagulant aid. *Indian J Environ Health*. 1962;4:233–44.
- Shubo D, Renbi B, Chen JP, et al. Produced water from polymer flooding process in crude oil extraction: characterization and treatment by a novel crossflow oil–water separator. *Sep Sci Technol*. 2002;29:207–16.
- Stuart BH. *Infrared spectroscopy: fundamentals and application*. Hoboken: Wiley; 2004. p. 71–93.
- Sutherland JP. Process for preparing coagulants for water treatment. US Patent, 6,890,565, 10 May 2005.
- Tatsi AA, Zouboulis AI, Matis KA, et al. Coagulation–flocculation pretreatment of sanitary landfill leachates. *Chemosphere*. 2003;53(7):737–44.
- Tripathi PN, Chaudhari M, Bokil SD. Nirmali seed—a naturally occurring coagulant. *Indian J Environ Health*. 1976;18:272–81.
- Ugonabo VI, Menkiti MC, Onukwuli OD. Effect of coag-flocculation kinetics on telfairia occidentalis seed coagulant (TOC) in pharmaceutical wastewater. *Int J Multidiscip Sci Eng*. 2012;9:22–33.
- Ugurlu M, Gurses A, Doğar M, et al. The removal of lignin and phenol from paper mill effluents by electrocoagulation. *J Environ Manag*. 2008;87:420–8.
- Verma S, Prasad B, Mishra I. Pretreatment of petrochemical wastewater by coagulation and flocculation and the sludge characteristics. *J Hazard Mater*. 2010;178:1055–64.
- von Smoluchowski M. Versuch einer mathematischen Theorie der Koagulationskinetik kolloider Lösungen. *Z Phys Chem*. 1917; 92:129–68.
- Vyazovkin S. *Thermogravimetric analysis. Characterization of materials*. 2nd ed. New York: Wiley; 2012. p. 1–12.
- Wang J, Qu C, Liu S. Progress in the development and application of oil field produced water treatment processes. *Appl Mech Mater*. 2014;641–642:376–9.
- Wei JC, Gao BY, Yue QY, et al. Performance and mechanism of polyferric-quaternary ammonium salt composite flocculants in treating high organic matter and high alkalinity surface water. *J Hazard Mater*. 2009;165:789–95.
- Yang Z, Gao B, Yue Q. Coagulation performance and residual aluminum speciation of $Al_2(SO_4)_3$ and polyaluminum chloride (PAC) in Yellow River water treatment. *Chem Eng J*. 2010;165:122–32.
- Zhao G, Ma F, Wei L, et al. Using rice straw fermentation liquor to produce bioflocculant during an anaerobic dry fermentation process. *Bioresour Technol*. 2012;113:83–8.
- Zheng Z, Zhang H, He PJ, et al. Co-removal of phthalic acid esters with dissolved organic matter from landfill leachate by coagulation and flocculation process. *Chemosphere*. 2009;75:180–6.
- Zhu G, Zheng H, Zhang Z, et al. Characterization and coagulation–flocculation behavior of polymeric aluminum ferric sulfate (PAFS). *Chem Eng J*. 2011;178:50–9.